J. Phys. D: Appl. Phys. 30 (1997) 1710–1719. Printed in the UK PII: S0022-3727(97)80324-5

# Adhesion mechanics of the surface force apparatus

**I Sridhar, K L Johnson and N A Fleck**

Cambridge University Engineering Department, Trumpington Street, Cambridge CB2 1PZ, UK

Received 17 December 1996

**Abstract.** The surface force apparatus (SFA) comprises thin molecularly smooth mica sheets glued to glass cylinders, which are pressed into contact with their axes at right angles. It is frequently used, in conjunction with the Johnson–Kendall–Roberts (JKR) adhesion theory, to extract the surface energy of the contacting sheets. This procedure is open to possible error since the JKR theory is based on the contact of homogeneous, isotropic elastic cylinders. This paper extends the JKR theory to the layered structure of the SFA. Two approaches have been followed: (i) direct calculations for prescribed values of the layer thickness and elastic moduli; (ii) an experimental calibration procedure for an existing apparatus.

## 1. Introduction

The surface force apparatus (SFA) was developed by Tabor and Winterton (1969) and Israelachvili and Tabor (1972). It comprises thin sheets of molecularly smooth mica, or similar material, glued to cylindrical glass lenses of equal radii, which are then pressed into elastic contact with their axes at right angles. A Hertz-type circular area of contact ensues whose radius $a$ can be measured by direct observation through the glass, glue and mica. The mica surfaces may be 'dry' or separated by molecularly thin films of fluid. In view of the smooth and intimate nature of the contact, adhesive forces are easily detectable, so that an important use of the apparatus lies in the measurement of surface energy (e.g. Israelachvili 1991, Mangipudi *et al* 1994).

In the presence of adhesive forces the contact size is larger than would be predicted by the Hertz theory; contact is maintained at zero applied load and a tensile force—the 'pull-off' force $P_c$—is needed to cause the surfaces to snap apart. In a typical experiment the contact size decreases as the load is reduced from a compressive (positive) to a tensile (negative) value until pull-off occurs. In order to deduce surface energies from such observations it is necessary to fit the measurements to an appropriate continuum mechanics model of the process. The so-called JKR theory (Johnson, Kendall and Roberts 1971) is commonly used for this purpose. It is asymptotically correct when the elastic deformation caused by the surface forces is large compared with their effective range of action. This condition is satisfied when the parameter (Tabor 1977):

$$\mu \equiv \left(\frac{Rw^2}{E^{*2}z_0^2}\right)^{1/3}$$

exceeds a value of about five, where $R$ = radius of each crossed cylinder, $E^*$ = effective elastic modulus, $z_0$ = equilibrium separation of the surfaces and $w$ = work of adhesion, i.e. $w = \Delta\gamma = \gamma_1 + \gamma_2 - \gamma_{12}$, where $\gamma_1$ and $\gamma_2$ are the surface energies of each surface and $\gamma_{12}$ that of the interface. In the SFA the low elastic modulus of the glue between the mica and glass generally ensures that the above condition is amply satisfied with $\mu \gg 5$.

However a problem arises with the effective modulus $E^*$. The JKR theory is based on the elastic analysis of two homogeneous and isotropic half-spaces with unequivocal elastic constants: Young's moduli $E_1$ and $E_2$, and Poisson's ratios $\nu_1$ and $\nu_2$ whereupon $E^* = [(1-\nu_1^2)/E_1 + (1-\nu_2^2)/E_2]^{-1}$. The contacting solids in the SFA, on the other hand, comprise layers having widely different elastic constants. Under load, as the contact size increases in relation to the (fixed) thickness of the layers, the effective modulus of the system changes. At a sufficiently light load the compliance will be that of the superficial mica sheet; with increasing load and contact size, the compliance will be increasingly dominated by the glue and subsequently the glass substrate.

This paper seeks to extend the JKR adhesion theory to a layered elastic system. Two separate approaches are followed. In the first approach it is assumed that the thickness of the layers and their individual elastic constants (taken to be isotropic) are known at the outset. In practice, however, this information is seldom known precisely, particularly in relation to the layer of glue. In the second approach a procedure is proposed for calibrating the apparatus *in situ* to find the *effective* modulus $E_e^*$ as a function of contact radius $a$. In this approach no knowledge of the thickness or moduli of the layers is required, but it must be possible to (i) modify the surfaces during calibration so that adhesion between them is negligible and (ii) to be able to measure both the size and *compliance* of the contact.

0022-3727/97/121710+10$19.50 © 1997 IOP Publishing Ltd

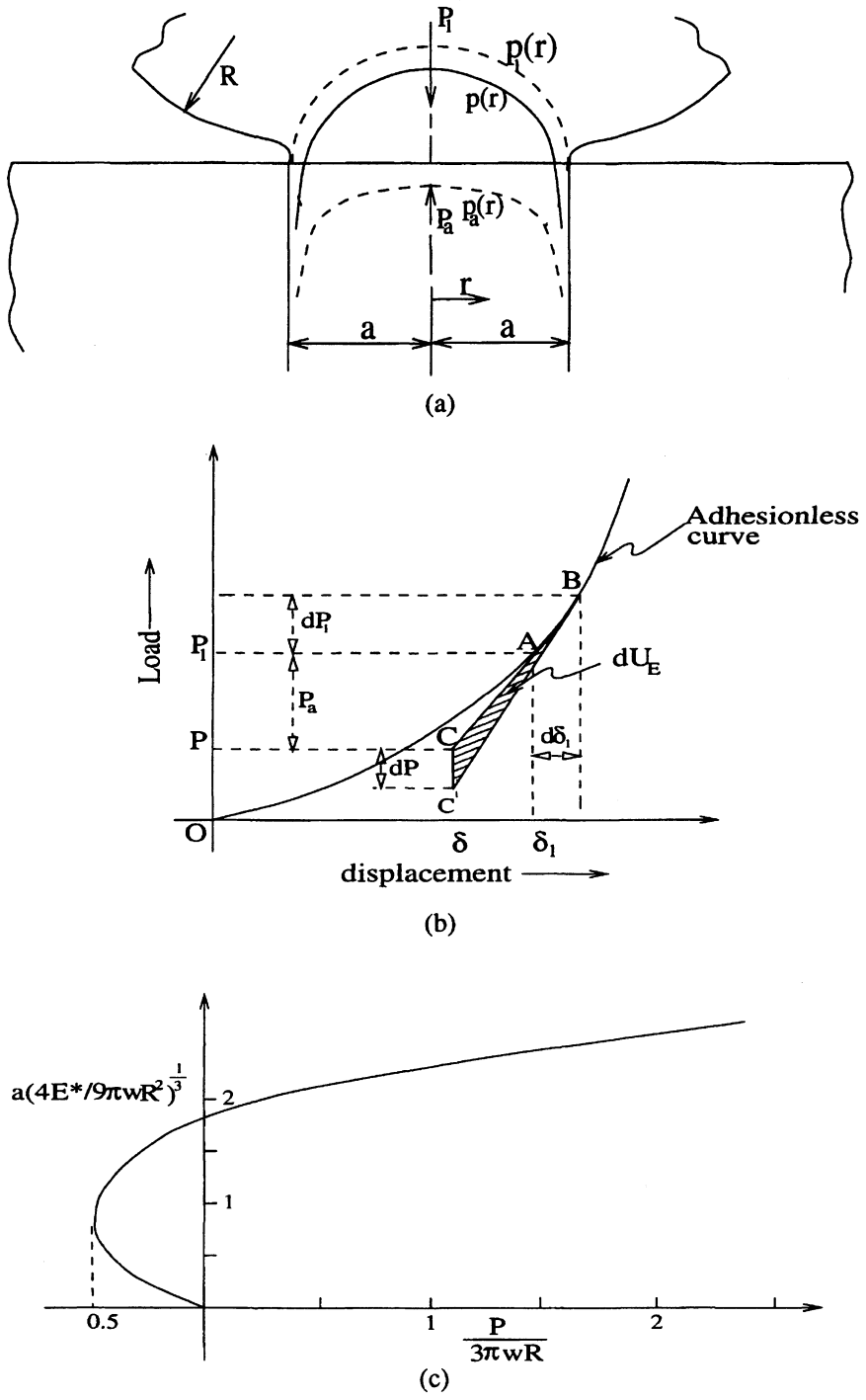


**Figure 1.** The JKR theory. (a) Contact pressure $p(r)$ is made up of two terms: Hertz pressure $p_1(r)$ and adhesion traction $p_a(r)$. (b) Relation between load $P$ and displacement $\delta$: application of $P_1$ – – – OA; application of $P_a$ – – – AC. (c) Variation of contact radius with load (equation (10)).

## 2. The JKR theory

A brief outline of the JKR elastic half-space theory will be presented as a starting point for the analysis of the layered system. Within the approximations of the Hertz theory the contact of two identical crossed cylinders is equivalent to the contact of a rigid frictionless sphere of the same radius with a plane surface of modulus $E^*$. The normal load is made up of two terms (see figure 1(a)): (i) an adhesionless load $P_1$ associated with the Hertz pressure

$$p_1(r) = \frac{3P_1}{2\pi a^2}\left[1 - \left(\frac{r}{a}\right)^2\right]^{1/2} \tag{1}$$

and (ii) an adhesive load $P_a$ associated with the pressure:

$$p_a(r) = -\frac{P_a}{2\pi a^2}\left[1 - \left(\frac{r}{a}\right)^2\right]^{-1/2} \tag{2}$$

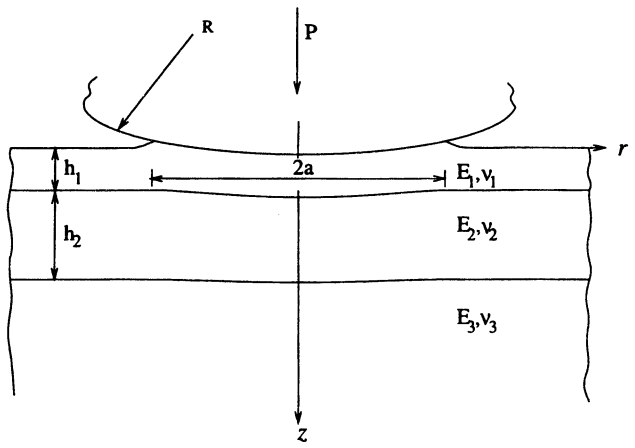


**Figure 2.** Indentation of a three-layer half-space by a smooth rigid sphere with adhesion.

which will be recognized to be that due to a flat punch of radius $a$. The superposition of these two tractions is shown in figure 1(a), and the net contact load $P = P_1 - P_a$. A plot of load against displacement $\delta$ is shown in figure 1(b). The application of the load $P_1$ in the absence of adhesion follows the compliance curve from $O$ to $A$. The adhesive (negative) force $P_a$ is then applied, keeping the contact size $a$ constant, which results in the linear compliance relation $AC$, having the gradient $(\mathrm{d}P_1/\mathrm{d}\delta_1)_A$. The Helmholtz free energy $U_T$ of the system may be expressed by

$$U_T = U_E + U_S$$

where $U_E$ is the elastic strain energy in the system at point $C$ in figure 1(b), and $U_S$ is the surface energy associated with a contact of radius $a$, i.e. $U_S = -\pi a^2 \Delta\gamma = -\pi a^2 w$. The equilibrium value of $a$ is then given by

$$\frac{\mathrm{d}U_T}{\mathrm{d}a} = \left(\frac{\partial U_E}{\partial a}\right)_\delta + \frac{\partial U_S}{\mathrm{d}a} = \left(\frac{\partial U_E}{\partial a}\right)_\delta - 2\pi a w = 0 \quad (3)$$

where the term $(\partial U_E/\partial a)_\delta$ is the rate of change of elastic energy with $a$, keeping the displacement $\delta$ constant ('fixed grips') and is shown by the shaded area CABC' in figure 1(b). In the limit:

$$\left(\frac{\mathrm{d}U_E}{\mathrm{d}a}\right)_\delta = \frac{1}{2}(\delta_1 - \delta)^2 \frac{\mathrm{d}}{\mathrm{d}a}\left(\frac{\mathrm{d}P_1}{\mathrm{d}\delta_1}\right)$$
$$= \frac{1}{2}\left(\frac{P_a}{\mathrm{d}P_1/\mathrm{d}\delta_1}\right)^2 \frac{\mathrm{d}}{\mathrm{d}a}\left(\frac{\mathrm{d}P_1}{\mathrm{d}\delta_1}\right). \quad (4)$$

Substituting in equation (3) gives

$$\frac{1}{4\pi a}\left[\frac{P_a}{\mathrm{d}P_1/\mathrm{d}\delta_1}\right]^2 \frac{\mathrm{d}}{\mathrm{d}a}\left(\frac{\mathrm{d}P_1}{\mathrm{d}\delta_1}\right) = w. \quad (5)$$

When the two contacting cylinders are homogeneous and isotropic (JKR theory) the Hertz relationships apply, so that the compliance curve in figure 1(b) is given by

$$P_1 = \frac{4E^* a^3}{3R} = \frac{4}{3}E^* R^{1/2}\delta_1^{3/2} \quad (6)$$

whereby

$$\frac{\mathrm{d}P_1}{\mathrm{d}\delta_1} = 2aE^*. \quad (7)$$

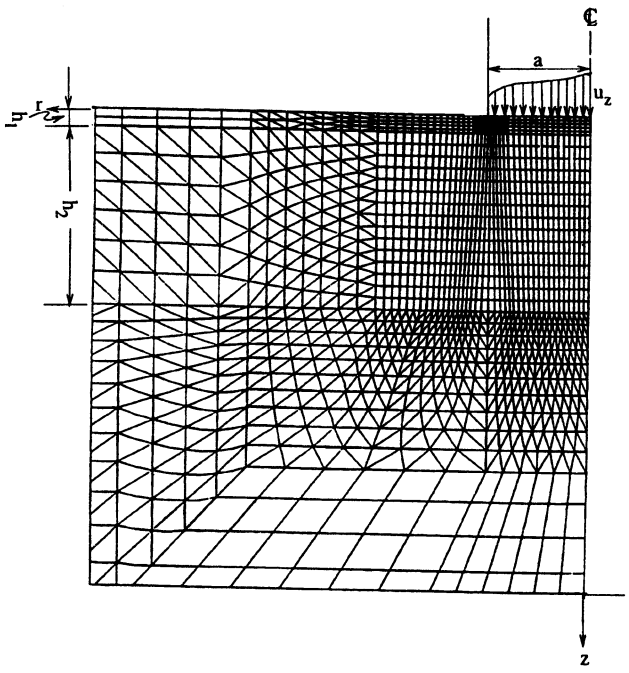


**Figure 3.** Axi-symmetric finite-element mesh for indentation of layered half-space.

Note that this contact stiffness is the same as that for a flat rigid punch. Substituting in equation (5) gives

$$P_a^2 = 8\pi w E^* a^3 \quad (8)$$

so that the net applied load is given by:

$$P = P_1 - P_a = \frac{4E^* a^3}{3R} - (8\pi a^3 w E^*)^{1/2}. \quad (9)$$

This is the JKR relationship between applied load $P$ and contact radius $a$. In non-dimensional variables $\bar{P} = P/3\pi w R$ and $\bar{a} = a(4E^*/9\pi w R^2)^{1/3}$ it reduces to

$$\bar{P} = \bar{a}^3 - \sqrt{2\bar{a}^3}. \quad (10)$$

The pull-off force can be shown to be $P_c = \frac{3}{2}\pi w R$.

An alternative approach to the JKR analysis is through the concepts of linear elastic fracture mechanics (Maugis and Barquins 1978). The singularity at $r = a$ in the adhesive traction of equation (2) can be expressed by a mode I stress intensity factor:

$$K_I = \frac{P_a}{2a\sqrt{\pi a}}. \quad (11)$$

For an equilibrium 'crack' the strain energy release rate is given by

$$G = \frac{K_I^2}{2E^*} = G_c = w. \quad (12)$$

Eliminating $K_I$ from (11) and (12) yields equation (8). Equation (12) and equation (5) respectively will form the bases of our two separate approaches to the analysis of adhesion in a layered system.

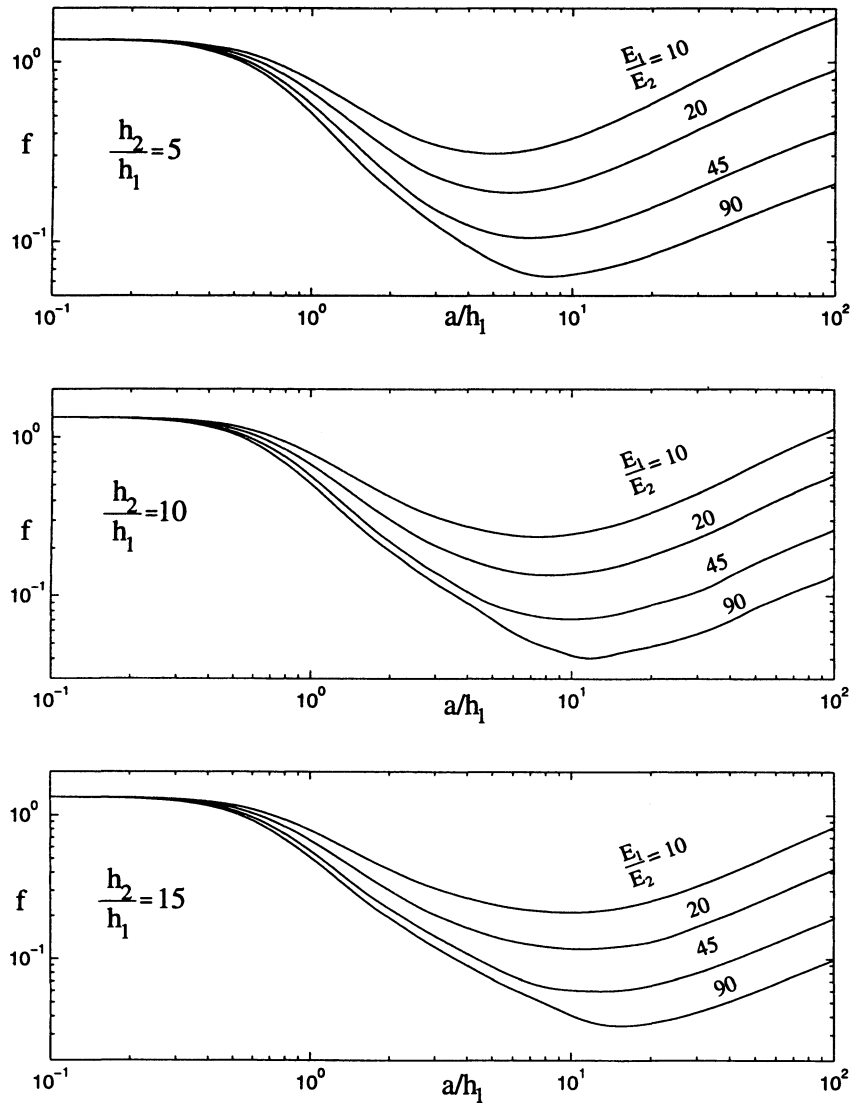


**Figure 4.** FE calculations of non-dimensional adhesionless load $f = (P_1 R/E_1^* h_1^3)$ as a function of contact size and other parameters (equation (13)).

## 3. Finite element analysis of layered system

The layered system is shown in figure 2. It comprises a substrate with superficial layers of thickness $h_1, h_2 \ldots$. The corresponding elastic constants of the layers and substrate are $E_i$ and $\nu_i$. The approach follows that of the JKR analysis: the superposition of the solution to an adhesionless contact and that of a flat rigid punch having the same contact size. In the layered system equation (6) for adhesionless contact (Hertz) may be rewritten in the form

$$\frac{P_1 R}{E_1^* a^3} = f\left\{\frac{a}{h_1}, \frac{h_2}{h_1}, \ldots \frac{E_2^*}{E_1^*}, \frac{E_3^*}{E_1^*}, \ldots\right\}. \tag{13}$$

In the case of the flat punch, equation (11) becomes

$$\frac{P_a}{K_I a^{3/2}} = g\left\{\frac{a}{h_1}, \frac{h_2}{h_1}, \ldots \frac{E_2^*}{E_1^*}, \frac{E_3^*}{E_1^*}, \ldots\right\}. \tag{14}$$

Substitution for $K_I$ in terms of $w$ from equation (12) gives

$$\frac{P_a R}{E_1^* a^3} = \left(\frac{2wR^2}{E_1^* h_1^3}\right)^{1/2} \left(\frac{h_1}{a}\right)^{3/2} g\left\{\frac{a}{h_1}, \frac{h_2}{h_1}, \ldots \frac{E_2^*}{E_1^*}, \frac{E_3^*}{E_1^*}, \ldots\right\}$$

$$= \left(\frac{2wR^2}{E_1^* h_1^3}\right)^{1/2} \bar{g}\left\{\frac{a}{h_1}, \frac{h_2}{h_1}, \ldots \frac{E_2^*}{E_1^*}, \frac{E_3^*}{E_1^*}, \ldots\right\}. \tag{15}$$

The net applied load $P$ is then given, as before, by

$$\frac{PR}{E_1 a^3} = \frac{P_1 R}{E_1 a^3} - \frac{P_a R}{E_1 a^3} = f - \alpha \bar{g} \tag{16}$$

where $\alpha \equiv (2wR^2/E_1 h_1^3)^{1/2}$ is a non-dimensional measure of the strength of adhesion. When $w = 0, \alpha = 0$ and equation (16) reverts to the adhesionless case expressed by equation (13). For any specific geometry and elastic constants the functions $f(a/h_1)$ and $\bar{g}(a/h_1)$ are evaluated by finite element analysis as described below.

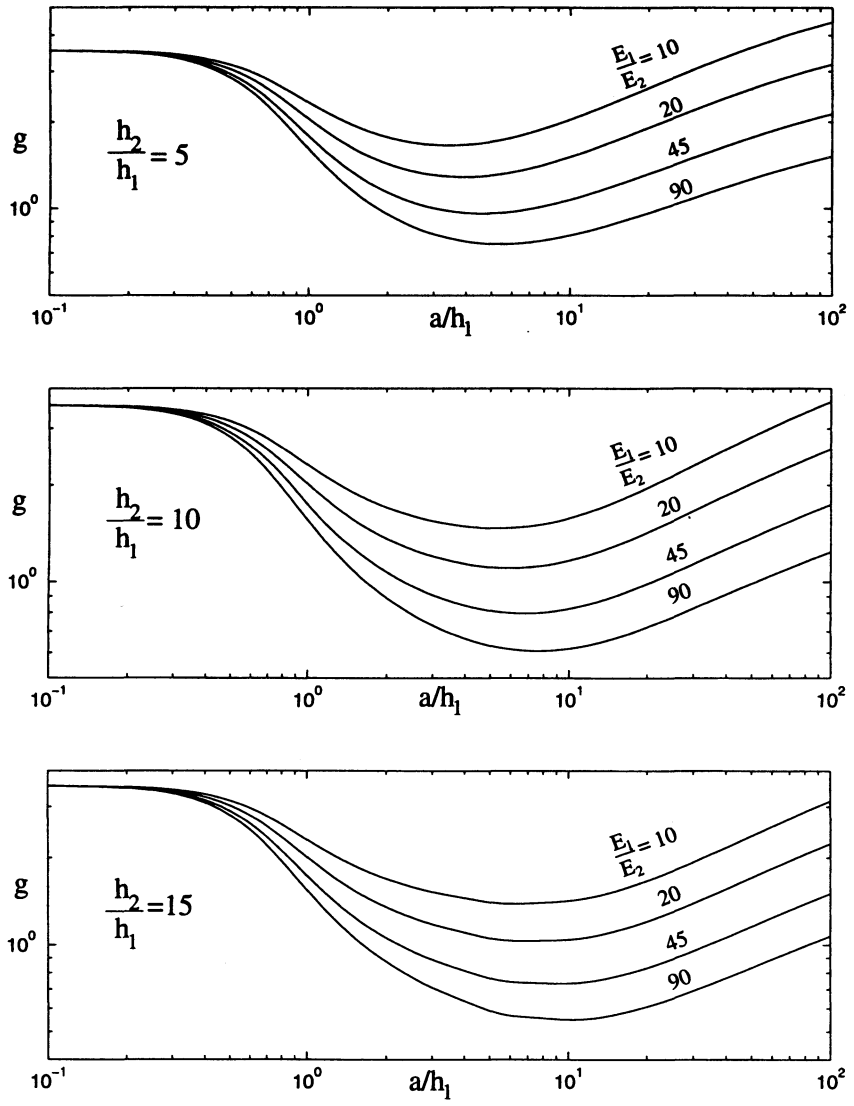


**Figure 5.** FE calculations of the non-dimensional adhesion force $g = (P_a/K_1 h_1^{3/2})$ as a function of contact size and other parameters (equation (14)).

The ABAQUS† finite element (FE) program is used for the linear elastic numerical analysis of the system shown in figure 2. The FE mesh and far-field boundary conditions are shown in figure 3. The layers are taken to be perfectly bonded. A large domain, 100–150 times the contact radius, is discretized using axi-symmetric 8-noded quadratic and 6-noded triangular elements. A particularly fine mesh is required in the region close to the edge of contact radius $r = a$ in order to obtain reliable values of the stress intensity factor $K_I$ at that point. Stresses at the remote boundaries are negligible.

To simulate indentation, the normal displacement

$$u_z(r) = \delta - \frac{r^2}{2R} \qquad \text{on } (r \leq a) \tag{17}$$

is decomposed into $u_z' = \delta$ and $u_z'' = -r^2/2R$, and applied separately. In non-dimensional form $u_z$ reads:

$$\frac{Ru_z}{a^2} = \frac{R\delta}{a^2} - \frac{1}{2}\left(\frac{r}{a}\right)^2 \tag{18}$$

† ABAQUS, HKS Inc., Rhode Island, USA.

The displacements in equation (17) give rise to loads $P'$ and $P''$ and to stress intensity factors $K_I'$ and $K_I''$ at $r = a$. The loads are found by summing the reaction forces at the nodes lying within the contact area. The stress intensity factors were found by an extension of the method due to Parks (1974) and Li *et al* (1985), which is described in appendix I. The displacement $u_z'(r)$ is that due to a flat punch in which the displacement $\delta'$, the load $P'$ and the stress intensity $K_I'$ are in direct proportion. In an adhesionless contact there is no singularity at $r = a$, so that $K_I' + K_I'' = 0$, whereupon the adhesionless load $P_1$ is given by:

$$P_1 = P'' - \left(\frac{K_I''}{K_I'}\right) P'. \tag{19}$$

Computing $P_1$ by equation (19) for a series of values $a/h_1$ yields the function $f(a/h_1)$. The function $g(a/h_1)$ is given directly by:

$$\frac{P_a}{K_I a^{3/2}} = \frac{P'}{K_I' a^{3/2}} = g\left(\frac{a}{h_1}\right). \tag{20}$$

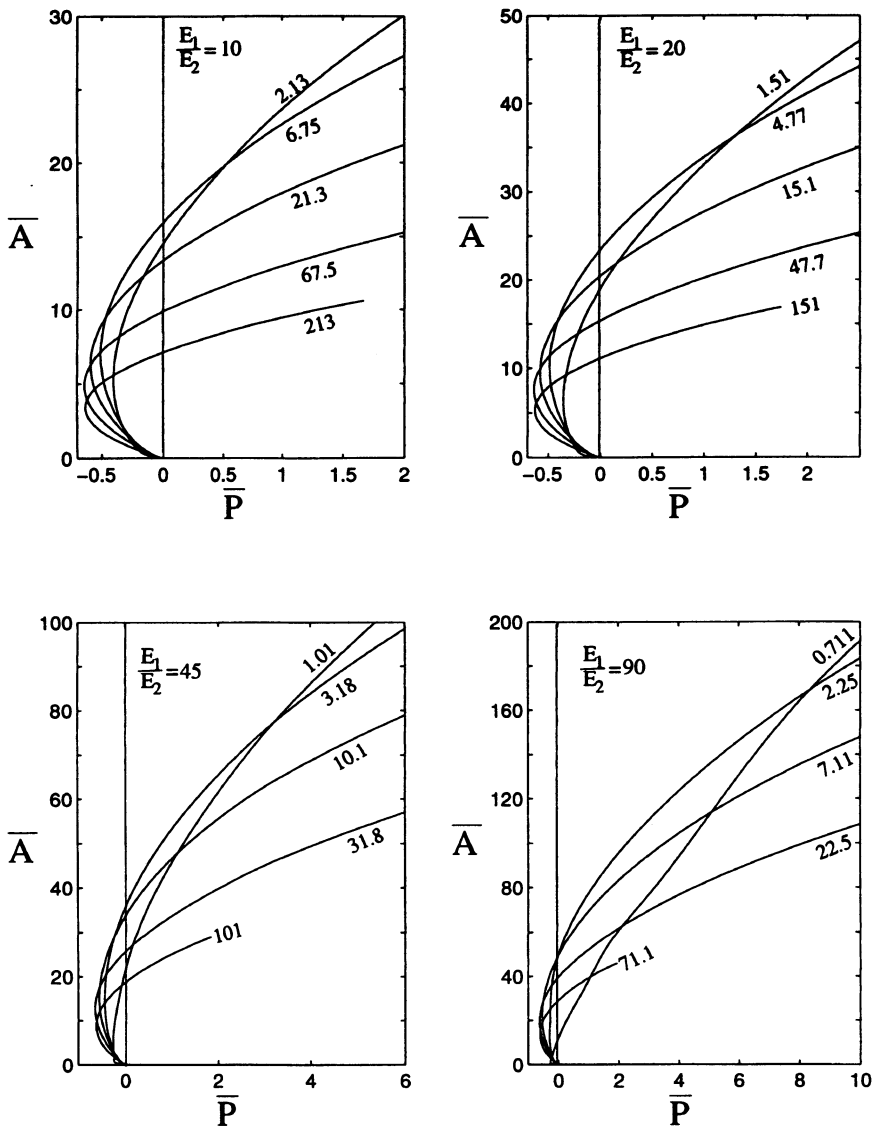


**Figure 6.** Variation of non-dimensional contact area $\bar{A} = \pi\bar{a}^2$ as a function of non-dimensional load $\bar{P} = P/3\pi wR$, for a range of values of the non-dimensional work of adhesion $\alpha = (2wR^2/E_1^* h_1^3)^{1/2}$, for the case $h_2/h_1 = 10$.

### 3.1. Numerical results

Finite element calculations have been carried out for a three-layer system representing a thin hard surface layer such as mica attached to a glass substrate with epoxy glue. Guided by the characteristics of the SFA used by Israelachvili (1991), the thickness of the layers and their elastic properties used in the computations are given in table 1. The radius $R$ of the cylinders was taken to be 20 mm and the contact radius was varied through the range 0.01–200 $\mu$m, but the presentation of results does not restrict their applicability to the *absolute* parameter values used in the calculations and quoted in table 1.

The functions $f(a/h_1)$ and $g(a/h_1)$ are plotted in figures 4 and 5 for various values of $h_2/h_1$, $E_2^*/E_1^*$ and $E_3^*/E_1^*$. For $a/h_1 < 0.3$ deformation is confined to the surface layer and $f(a/h_1)$ takes the value 4/3 given by equation (6). With increasing indentation size, $f(a/h_1)$ decreases in response to the compliance of the layer of glue, until the stiffening provided by the glass substrate becomes significant. A similar variation is found in the function $g(a/h_1)$.

The net load $P(= P_1 - P_a)$ is obtained from the functions $f$ and $\bar{g}$ by equation (16) with $\alpha$ as a parameter. Transforming (16) to the JKR variables defined in equation (10) provides the relationship between the normalized load $\bar{P}$ and contact radius $\bar{a}$:

$$\bar{P} = \tfrac{3}{4}\bar{a}^3(f - \alpha\bar{g}). \tag{21}$$

Curves of contact area $\bar{A} = \pi\bar{a}^2$ plotted against load $\bar{P}$ are presented in figure 6. They are of the same general shape as the JKR curve (equation (10) and figure 1(c)): contact at zero load and a critical adhesive (negative) load $\bar{P}_c$, at pull-off, but showing wide variations in magnitude with adhesion parameter $\alpha$, layer thickness and moduli. The values of the normalized pull-off force $\bar{P}_c$ have been measured from the curves and plotted aganist $\alpha$ in figure 7. The adhesion parameter has a significant effect on $\bar{P}_c$, which ranges from zero to 0.62 compared with the JKR

**Table 1.** The parameter values used in calculations.

| Layer no | Material | Young's modulus (GPa) | Poisson's ratio | Layer thickness ($\mu$m) |
|---|---|---|---|---|
| 1 | mica | 10, 20, 90, 180 | 0.3 | 2 |
| 2 | epoxy glue | 2 | 0.4 | 10, 20, 30 |
| 3 | glass substrate | 70 | 0.2 | — |

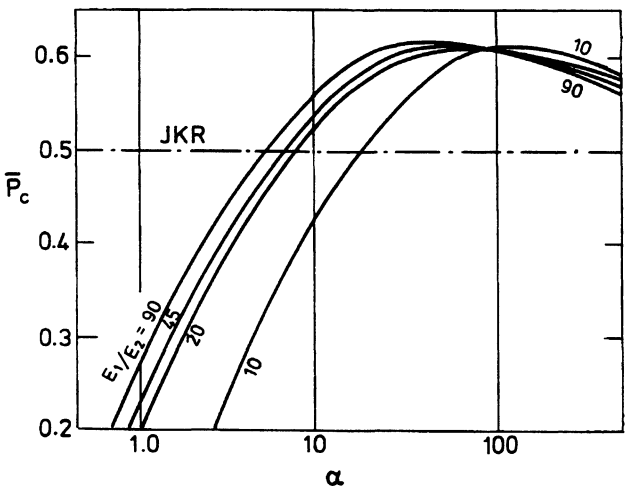


**Figure 7.** Non-dimensional pull-off force $\bar{P}_c = P/3\pi wR$ as a function of the non-dimensional work of adhesion $\alpha = (2wR^2/E_1^* h_1^3)^{1/2}$.

value of 0.5. The influence of layer thickness $h_2/h_1$ was found to be negligible within the numerical scatter. The effect of the modulus ratio $E_1^*/E_2^*$ is not large either, particularly for $E_1^*/E_2^* > 20$.

## 4. Experimental calibration of effective modulus

In this section we propose an experimental calibration of the effective elastic modulus of an existing apparatus, without prior knowledge of the thickness of the layers or moduli of the layer materials. The 'effective modulus' $E_e^*$ is defined as the modulus of a homogeneous isotropic half-space which would exhibit the same stiffness $\mathrm{d}P/\mathrm{d}\delta$ as the layered system. It is clearly a function of the contact size $a$.

In order to carry out this calibration it is necessary to modify the surfaces such that adhesion between them is negligible, and to be able to measure the approach of the two surfaces $\delta$ due to their elastic compression. In this way the adhesionless compliance curve, $P_1$ versus $\delta_1$, shown diagrammatically in figure 1(b), is obtained experimentally. Simultaneous measurements of the contact radius $a$ must also be made. By equation (8) we can then write:

$$E_e^*(a) = \frac{1}{2a}\frac{\mathrm{d}P_1}{\mathrm{d}\delta_1}. \tag{22}$$

Thus determination of $E_e^*$ requires differentiation of the experimental compliance curve. The accuracy of this process could be significantly improved if the technique were employed of applying an oscillating force of small amplitude to the contact to measure the derivative $(\mathrm{d}P_1/\mathrm{d}\delta_1)$ directly (Pethica and Oliver 1987, Georges *et al* 1993).

To demonstrate the validity of this procedure we have evaluated $E_e^*(a/h_1)$ from equation (22) by numerical differentiation of the compliance relationship $P_1(\delta)$ obtained from the FE computations. The results are shown by the points in figure 8. For comparison $E_e^*(a/h_1)$ has been calculated directly from the FE computations of indentation by a flat punch, for which $\mathrm{d}P_1/\mathrm{d}\delta_1 = P'/\delta'$, shown by the full curves in figure 8. It is recognized, of course, that differentiation of an experimental compliance curve will show more scatter than our numerical results, but the calibration procedure outlined above is a 'once and for all' experiment on any given apparatus, and can therefore be carried out with care and thoroughness.

The behaviour during an adhesion experiment follows from equation (6). Substituting from equation (22) into (6) gives

$$P_a^2 = (P_1 - P)^2 = 8\pi w a^3 E_e^*(a)\left[1 + \frac{a}{E_e^*}\left(\frac{\mathrm{d}E_e^*}{\mathrm{d}a}\right)\right]^{-1}. \tag{23}$$

$P(a)$ is found from an adhesion experiment having the form illustrated in figure 6; $P_1(a)$ is obtained from the adhesionless calibration experiment. The work of adhesion $w$ (or $\Delta\gamma$) is then obtained by fitting the results to equation (23). It will be seen that equation (23) requires a further differentiation. Values of the product $(a/E_e^*)(\mathrm{d}E_e^*/\mathrm{d}a)$ obtained from numerical differentiation of our results given in figure 8 are shown in figure 9. It is evident that the second term in the bracket in equation (23) is small for $1 < a/h_1 < 10$, i.e. in the region where it crosses the axis. This is the range where the assumption of constant $E_e^*$, obtained by the usual procedure of fitting the JKR curve (equation (10)), would involve least error.

## 5. Conclusions

Adhesion of the system of elastic layers used in the SFA has been analysed and compared with the JKR analysis for a homogeneous isotropic half-space. The adhesion characteristics, including the pull-off force, depend upon an adhesion parameter $\alpha = (2wR^2/E_1^* h_1^3)^{1/2}$ as well as on the ratio of thickness of the layers $h_2/h_1$, and the ratio of their elastic moduli $(E_1^*/E_2^*)$ and $(E_1^*/E_3^*)$.

Two approaches to the problem have been considered.

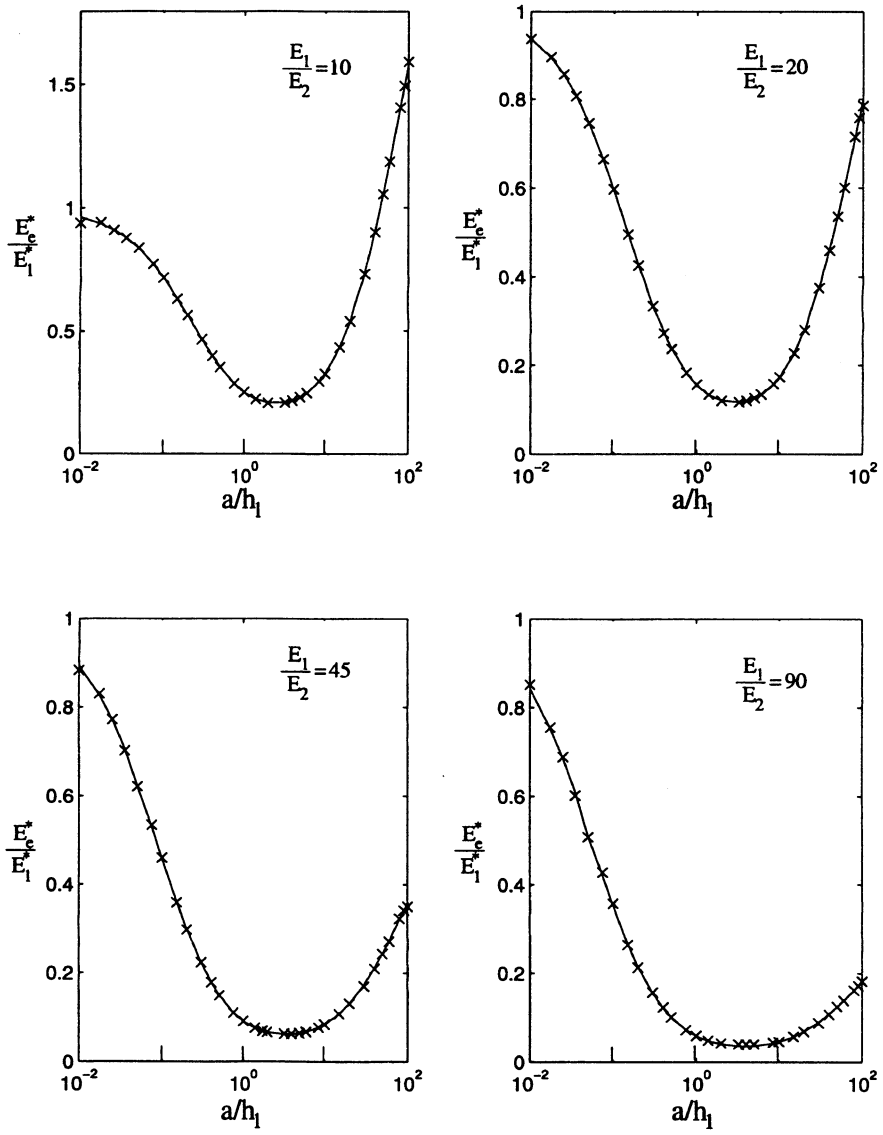


**Figure 8.** Effective elastic modulus $E_e^*$ for the case $h_2/h_1 = 10$. Curves from the FE flat punch solution; points from the gradient $(dP_1/d\delta_1)$ of adhesionless compliance curve.

(i) FE analysis of the system where the thicknesses and elastic moduli of the layers are known in advance. Results are presented for varying $(h_2/h_1)$, $(E_1^*/E_2^*)$ and $(E_1^*/E_3^*)$, from which required values can be interpolated. The pull-off force $P_c$ is found to depend critically upon the adhesion parameter $\alpha$, but not to a large extent upon the thickness or moduli ratios.

(ii) An experimental calibration of the compliance of the apparatus is proposed, in which it is necessary to measure the contact area and the compression of the system under condition of zero adhesion. It is shown that maximum accuracy of the calibration would be expected by carrying out the experiment in the range of contact size $1.0 < a/h_1 < 10.0$, for the practical range of the moduli and thickness ratios.

In circumstances where the JKR relationship is used as an approximate fit to the results of an adhesion experiment, minimum errors would arise if the contact size $a/h_1$ were chosen to lie in the range where $(a/E_e^*)(dE_e^*/da)$ is small.

## Appendix. Determination of energy release rate *G*

The energy release rate at the edge of the indenter is determined from the finite element solution by making use of a virtual crack extension method, as developed by Parks (1974) and extended by Li *et al* (1985). A brief summary of the implementation is given below.

Consider the state in the surface elastic layer and introduce local co-ordinates $(x_1, x_2)$ centred at the edge of the contact, as shown in figure 10(a). The strain energy release rate $G$ at the contact edge is given by the $J$-integral:

$$G = J \equiv \int_{\Gamma_0} \left( W n_1 - \sigma_{ij} n_i \frac{\partial u_j}{\partial x_1} \right) ds \qquad \text{(A1)}$$

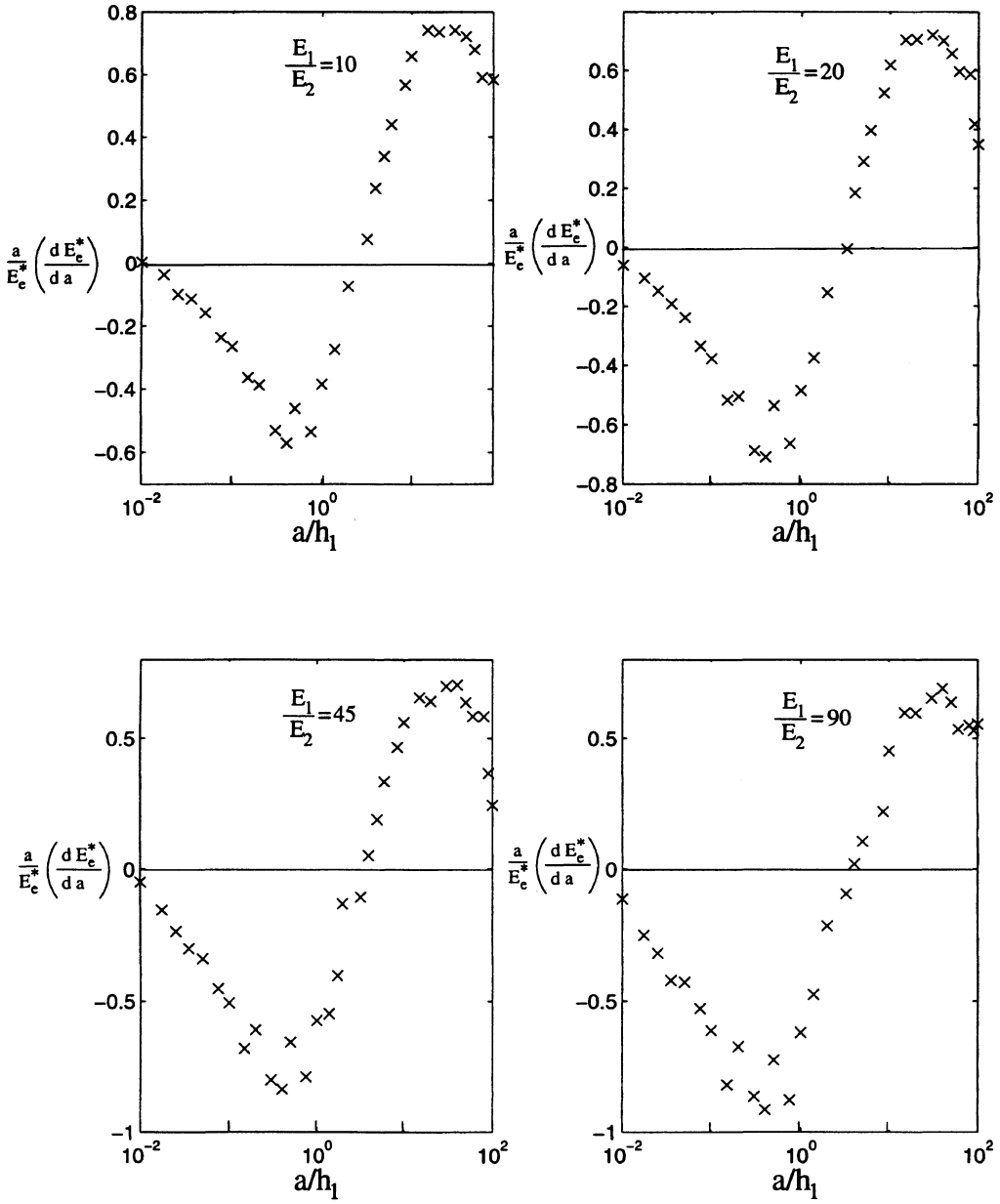


**Figure 9.** The correction term $(a/E_e^*)(\mathrm{d}E_e^*/\mathrm{d}a)$ in equation (23) for the variation in effective modulus $E_e^*$ with contact size, derived from the gradient of the curves in figure 8, $(h_2/h_1 = 10)$.

where $\Gamma_0$ is any path which begins on the surface of the solid at a vanishing distance outside the contact edge, and ends on the surface of the solid at a vanishing distance inside the contact edge. Here $n_i$ is the outward normal to $\Gamma_0$, $\sigma_{ij}$ is the stress, $u_i$ is the displacement, $\mathrm{d}s$ is the arc length along $\Gamma_0$ and $W$ is the strain energy density defined by

$$W(\epsilon_{kl}) = \int_0^{\epsilon_{kl}} \sigma_{ij}\, \mathrm{d}\epsilon_{ij} \tag{A2}$$

Note that the value of $J$ is path independent such that the integral defined in (A1) vanishes for any closed path excluding a singularity. Accurate numerical estimates of $J$ are best obtained by converting the contour integral (A1) into a domain integral at a distance of several finite elements from the contact edge. Parks' method, in essence, is this domain integral technique. The transformation is carried out in two steps.

(i) Path independence of the $J$-integral allows (A1) to be re-written as

$$J = \int_{\Gamma_1+\Gamma_2+\Gamma_3} \left(Wn_1 - \sigma_{ij}n_i\frac{\partial u_j}{\partial x_1}\right)\mathrm{d}s$$
$$= \int_{\Gamma_2} \left(Wn_1 - \sigma_{ij}n_i\frac{\partial u_j}{\partial x_1}\right)\mathrm{d}s + \int_{\Gamma_3} \left(-\sigma_{ij}n_i\frac{\partial u_j}{\partial x_1}\right)\mathrm{d}s \tag{A3}$$

where the various contours are defined in figure 10(b). In (A3), use has been made of the fact that $n_1$ vanishes on $\Gamma_1$ and $\Gamma_3$, and that $\Gamma_1$ is traction free.

(ii) With reference to figure 10(c) it is convenient to re-write the integral over $\Gamma_2$ in (A3) in the form of a closed

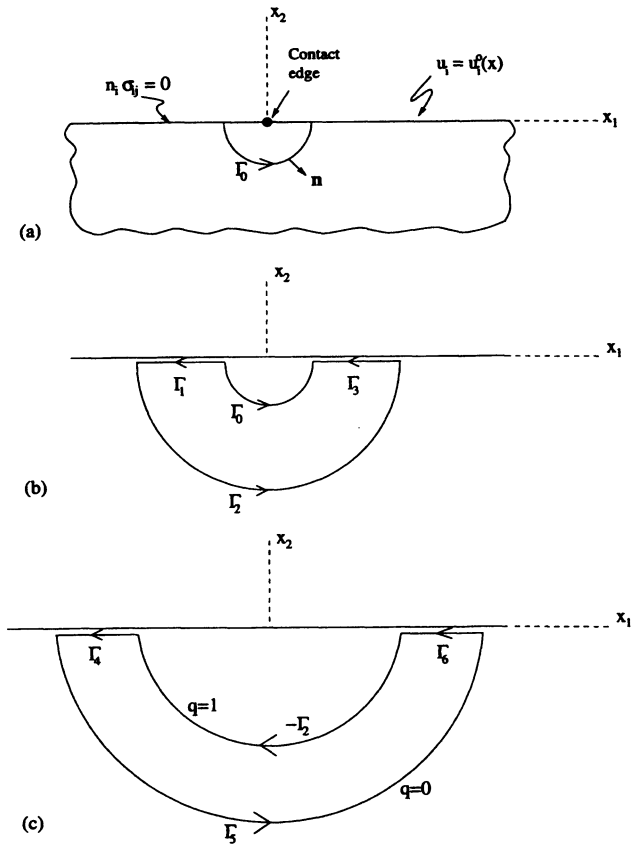


**Figure 10.** Contour integrals used in the evaluation of the $J$-integral.

contour:

$$\int_{\Gamma_2}\left(Wn_1-\sigma_{ij}n_i\frac{\partial u_j}{\partial x_1}\right)\mathrm{d}s$$
$$=-\oint_{\Gamma_4+\Gamma_5+\Gamma_6-\Gamma_2} q\left(Wn_1-\sigma_{ij}n_i\frac{\partial u_j}{\partial x_1}\right)\mathrm{d}s$$
$$+\int_{\Gamma_4} q\left(Wn_1-\sigma_{ij}n_i\frac{\partial u_j}{\partial x_1}\right)\mathrm{d}s$$
$$+\int_{\Gamma_5} q\left(Wn_1-\sigma_{ij}n_i\frac{\partial u_j}{\partial x_1}\right)\mathrm{d}s$$
$$+\int_{\Gamma_6} q\left(Wn_1-\sigma_{ij}n_i\frac{\partial u_j}{\partial x_1}\right)\mathrm{d}s \qquad \text{(A4)}$$

where the scalar function $q(x)$ is given the value $q=1$ on $\Gamma_2$, $q=0$ on $\Gamma_5$ and is taken to vary linearly with $s$ over $\Gamma_4$ and $\Gamma_6$. The fourth term on the right-hand side of (A4) vanishes since the integrand vanishes over $\Gamma_5$. The second term on the right-hand side of (A4) also vanishes since $n_1=\sigma_{ij}n_j=0$ on $\Gamma_4$. On collecting the remaining terms in (A3) and (A4), the $J$-integral may be expressed as

$$J=-\oint_{\Gamma_4+\Gamma_5+\Gamma_6-\Gamma_2} q\left(Wn_1-\sigma_{ij}n_i\frac{\partial u_j}{\partial x_1}\right)\mathrm{d}s$$
$$+\int_{\Gamma_6+\Gamma_3}-q\left(\sigma_{ij}n_i\frac{\partial u_j}{\partial x_1}\right)\mathrm{d}s. \qquad \text{(A5)}$$

Parks (1974) and Li *et al* (1985) have shown that the closed contour integral specified in (A5) is precisely the energy release rate associated with a virtual decrease of the contact size by an amount $\delta a=-1$. The contact size is decreased by translating all nodes within $\Gamma_2$ of the finite element mesh by unity in the $x_1$-direction. All nodes outside the ring $\Gamma_5$ are held fixed, so that only the elements between the two contours are distorted. Following Parks (1974), the closed contour integral in (A5) can be re-written as

$$-\oint_{\Gamma_4+\Gamma_5+\Gamma_6-\Gamma_2} q\left(Wn_1-\sigma_{ij}n_i\frac{\partial u_j}{\partial x_1}\right)\mathrm{d}s$$
$$\equiv\frac{1}{2}\{u_n\}^T\frac{\partial \mathbf{S}}{\partial a}\{u_n\}. \qquad \text{(A6)}$$

The elements of the vector $\{u_n\}$ are the nodal displacements of the finite element calculation and [**S**] is the associated finite element stiffness matrix. The right-hand side of (A6) is calculated as follows. First, the indentation problem is solved in order to determine the values of $\{u_n\}$. Then, the nodes within and on the contour $\Gamma_2$ are displaced a small distance $\delta a=-1$ parallel to the $x_1$-direction; nodes on and outside of $\Gamma_5$ are simultaneously held fixed, and the stiffness matrix is recomputed. Note that [**S**] changes only for those elements placed between contours $\Gamma_2$ and $\Gamma_5$. The right-hand side of (A6) is then computed. The procedure is done automatically within the ABAQUS finite element package. Finally, the correction term given by the second term of the right-hand side of (A5) is used in the estimation of $G=J$.

## References


Georges J M, Millot S, Loubet J L and Tonk A 1993 *J. Chem. Phys.* **98** 7345

Israelachvili J N 1992 *Intermolecular Surface Forces* 2nd edn (San Diego, CA: Academic)

Israelachvili J N and Tabor D 1972 *Proc. R. Soc.* A **331** 19–38

Johnson K L, Kendall K and Roberts A D 1971 *Proc. R. Soc.* A **324** 301–13

Li F Z, Shih C F and Needleman A 1985 *Eng. Frac. Mech.* **21** 405–21

Mangipudi V, Tirrell M and Pocius A V 1994 *J. Adhesion Sci. Technol.* **8** 1251–70

Maugis D and Barquins M 1978 *J. Phys. D: Appl. Phys.* **11** 1989–2023

Parks D M 1974 *Int. J. Fracture* **10** 487–502

Pethica J B and Oliver W C 1987 *Phys. Scr.* T **19** 61–6

Tabor D 1976 *J. Coll. Interface Sci.* **58** 1–13

Tabor D and Winterton R H S 1969 *Proc. R. Soc.* A **312** 435